Int. J. Heat Mass Transfer. Vol. 28, No. 5, pp. 939–947, 1985
Printed in Great Britain

0017–9310/85 $3.00 + 0.00

A note on the loop thermosyphon with mixed boundary conditions

J. E. HART
Department of Astrophysical, Planetary and Atmospheric Sciences,
University of Colorado, Boulder, CO 80309, U.S.A.

(*Received* 10 *August* 1984 *and in final form* 11 *November* 1984)

Abstract—This paper presents a one-dimensional model for flow in a toroidal fluid loop in which the wall heat transfer coefficient is constant over one half of the loop, and zero over the other. A mathematically low-dimensional form of the model gives reasonably accurate predictions of the steady state mass flow, stability, and the nature of non-steady motions. Numerical computations with a high-dimensional model illustrate the effects of mixed boundaries and axial heat conduction on the chaotic solutions. Comparisons are made with previous low-dimensional models that are exact only for a spatially uniform heat transfer coefficient.

1. INTRODUCTION

THERE HAS recently been considerable interest in convective flows in closed fluid loops, both as examples of simple systems that display complex dynamical behavior, and as systems of practical interest in a diverse range of applications. Malkus [1] showed that under certain symmetry constraints the partial differential equations describing the cross-sectionally averaged flow in a toroidal thermosyphon, with temperatures imposed at the boundaries and heating from below, could be reduced to the three-component Lorenz [2] equations. Hart [3] proposed a similar model for flow in a loop but included power-law friction and a more general heating function with internal volumetric and boundary wall fluxes. The boundary heating distribution could be rotated away from the vertical axis defined by gravity. It was stated in [3] that the model applies to situations in which the heat transfer coefficient varies around the loop in a simple way, in addition to cases where the heat transfer coefficient is uniform. The former is an important situation since many of the published laboratory experiments on fluid loops (e.g. [4], [5] and [6]) have been carried out using a toroidal loop that has an isothermal (cooled) upper half-section and a wall-heated lower half-section, where the intent was for the lower wall to be an ideal flux boundary with no heat loss. The case with conducting walls (temperature boundary conditions around the whole loop) would also seem to be amenable to laboratory simulation, perhaps with better control on the boundary values (since it is difficult to construct an experiment with a true flux condition).

Sen (private communication, see also [7]) has indicated, correctly, that the three-component model of [3] is not exact when the heat transfer coefficient varies with angle around the loop. It is the purpose of this note to clarify this point and to indicate what changes in behavior are found when the model of [3] is generalized to include the case of mixed boundary conditions. In Section 2 the model equations are derived. A truncation is performed that reduces the full set of equations to a subset similar to the master problem equations of [3]. The reduced model gives a good prediction of the steady flow velocity, and indicates that there are multiple equilibria and chaotic solutions as found previously. Numerical integrations carried out using a high-order (convergent) truncation are described in Section 3. For the several cases studied, the bifurcation sets are nearly the same, but there are some subtle differences in the nature of the chaotic solutions. These and other properties of the model are summarized in Section 4.

2. FORMULATION

As in [3] we consider the flow of a Boussinesq liquid in the toroidal fluid loop shown in Fig. 1. Heat fluxes H or wall temperatures T_w are imposed around the periphery of the loop. When the inner radius R_p is small compared to the outer radius R_o the standard one-dimensional thermosyphon model is generated by cross-sectionally averaging the momentum, continuity, and thermal energy equations (see [3] or references cited therein for details). One arrives at the following equations

$$\frac{\rho\,\mathrm{d}v^*}{\mathrm{d}t^*} = \frac{g\rho\beta}{2\pi}\int_{-\pi}^{\pi}[\cos(\alpha)\cos(\theta)T^* - \sin(\alpha)\sin(\theta)T^*]\,\mathrm{d}\theta - \frac{2\tau}{R_p} \quad (1)$$

$$\rho C_p\frac{\mathrm{d}T^*}{\mathrm{d}t^*} \equiv \rho C_p\left(\frac{\partial T^*}{\partial t^*} + \frac{v^*}{R_o}\frac{\partial T^*}{\partial\theta}\right) = -2h(\theta)\frac{T^*-T_w}{R_p} + H(\theta) + \frac{k}{R_o^2}\frac{\partial^2 T^*}{\partial\theta^2}. \quad (2)$$

The angle α measures the rotation of the axis $\theta = 0$ with respect to the horizontal so that the boundary discontinuity (see below) and the heating can be inclined with respect to the gravity vector. The last term

NOMENCLATURE

A	non-dimensional measure of axial heat conduction
b	defined in equation (4e)
C_d	drag coefficient
C_p	specific heat at constant pressure
g	gravitational acceleration
h	wall heat transfer coefficient
h'	non-dimensional heat transfer coefficient, h/h_0
h_o	heat transfer scale $\equiv h(\theta = \pi/2)$
H	wall or internal heating function, see Fig. 1
k	thermal conductivity
K	truncation limit
Pr'	'Prandtl number', R_oC_d/R_p, see also equation (4c)
Ra'	'Rayleigh number' $\Delta T_d/\Delta T$, see also equation (4d)
R_o	radius of toroidal loop, Fig. 1
R_p	radius of fluid pipe, Fig. 1
t^*	time
t'	non-dimensional time, see also equation (4f)
t''	non-dimensional lag time
T^*	temperature fluctuation
T'	non-dimensional temperature fluctuation
T_d	non-dimensional thermal boundary forcing function
T_w	dimensional thermal forcing function, Fig. 1
v^*	cross-sectionally averaged circumferential velocity
v'	non-dimensional velocity
V	velocity scale, $2hR_o/R_pC_p$
X	non-dimensional circulation
y_0	fluctuating part of the azimuthal mean temperature
Y_0	steady part of the mean temperature
Y, Y_n	temperature amplitude functions
Z, Z_n	temperature amplitude functions.

Greek symbols

α	angle of torus boundary discontinuity with the horizontal plane
β	coefficient of thermal expansion
δ_{ij}	Kronecker delta
ΔT	temperature scale $2V^2C_d/g\beta R_p$
ΔT_d	forcing temperature scale
ρ	density
τ	wall stress
θ	azimuthal angle, Fig. 1.

Subscripts

n	index of Fourier expansion functions
m	summation index in cross-diffusion terms

in equation (2) represents axial heat diffusion with conductivity k. We take a linear drag law $\tau = 0.5C_dVv^*$ where C_d is the drag coefficient and $V = 2h_oR_o/\rho R_pC_p$ is a velocity scale. We also use the scale $\Delta T = 2V^2C_d/g\beta R_p$ for temperature, and the scale R_o/V for time. The parameter $h_o \equiv h(\pi/2)$ is taken as the scale for the heat transfer coefficient. With this non-dimensionalization and primes denoting non-dimensional variables, equations (1) and (2) become:

$$\frac{dv'}{dt'} = Pr'\left[-v' + \frac{1}{\pi} \times \int_{-\pi}^{\pi} \{\cos(\theta)\cos(\alpha)T' - \sin(\alpha)\sin(\theta)T'\}\, d\theta\right] \quad (3)$$

$$\frac{\partial T'}{\partial t'} + v'\frac{\partial T'}{\partial \theta} = -T'h'(\theta) + Ra'T_d(\theta) + A\frac{\partial^2 T'}{\partial \theta^2}. \quad (4)$$

We have introduced a non-dimensional thermal driving function T_d with scale ΔT_d, such that $\Delta T_d \times T_d = T_w(\theta) + R_pH(\theta)/2h_o$ is the net heating function. $Pr' = R_oC_d/R_p$ is essentially a Prandtl number, and $Ra' = \Delta T_d/\Delta T$ is a Rayleigh number (Hart [3]). The relative importance of axial diffusion is determined by $A \equiv kR_p/2R_o^2h$.

In this paper we specify $h' = 0$ for $-\pi < \theta < 0$, and $h' = 1$ for $0 <= \theta <= \pi$. In addition we consider the cooling temperature to be a constant ambient value, and without loss of generality set $T_w = 0$. We focus on the case with $T_d = 1$ for $-\pi < \theta < 0$ and zero otherwise, corresponding to uniform heating over

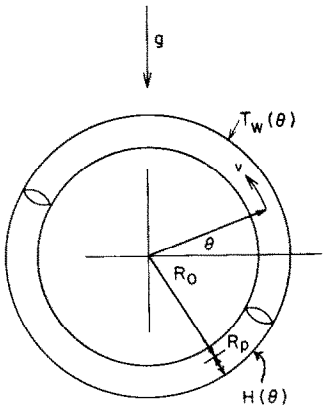

FIG. 1. Cross-section of the closed loop thermosyphon. The upper half ($\theta > 0$) has conducting walls, while on the lower half ($\theta < 0$) a heat flux is imposed. The $\theta = 0$ line can be rotated through an angle α (positive counter-clockwise) with respect to g.

the lower half of the torus. All this corresponds to the experimental conditions in refs. [4]–[6].

Following the method of [3] the partial differential equations are converted to a set of ordinary differential equations by a finite Fourier transform of the temperature field. Using the following transformations

$$v' = \frac{X(1+2A)}{2} \tag{4a}$$

$$T' = \frac{1+2A}{2}\left[\sum_{n=1}^{\infty}[Z_n \sin(n\theta) + Y_n \cos(n\theta)]\right] - \frac{(1+2A)Ra \sin(\theta)}{2} + (1+2A)\frac{Ra'}{\pi} + \frac{(1+2A)^2 \pi y_0}{8} \tag{4b}$$

$$Pr = \frac{2Pr'}{1+2A} \tag{4c}$$

$$Ra = \frac{16Ra'}{(1+2A)\pi b} \tag{4d}$$

$$b \equiv 1 - \frac{8}{\pi^2} \tag{4e}$$

$$t = \frac{(1+2A)t'}{2} \tag{4f}$$

with,

$$f_n = \frac{1+2n^2A}{1+2A}, \tag{5}$$

we obtain

$$\frac{dX}{dt} = Pr[-X + \cos(\alpha)Y_1 - \sin(\alpha)(Z_1 - Ra)] \tag{6}$$

$$\frac{dY_n}{dt} = -nXZ_n - Y_n f_n + Ra\, X\delta_{n1} + 2Ra\left[\frac{(-1)^n+1}{\pi(1-n^2)(1+2A)}\right]_{n<>1} + \sum_{m=1,<>n}^{\infty} \frac{2m[(-1)^{m+n}-1]Z_m}{(1+2A)\pi(m^2-n^2)} \tag{7}$$

$$\frac{dZ_n}{dt} = nXY_n - Z_n f_n + \frac{y_0[(-1)^n - 1]}{2n} + b\, Ra(1-\delta_{n1})\frac{(-1)^n - 1}{4(1+2A)\pi n} + \sum_{m=1,<>n}^{\infty} \frac{2n[(-1)^{m+n}-1]Y_m}{\pi(1+2A)(n^2-m^2)} \tag{8}$$

$$\frac{dy_0}{dt} = \frac{1}{1+2A}\left[-y_0 + \sum_{m=1}^{\infty} 4Z_m \frac{(-1)^m - 1}{m\pi^2(1+2A)}\right]. \tag{9}$$

These equations can be truncated at some large value of the index n. They can be arranged in a vector of length K, with the first component being equation (6), the last being equation (9), and the equations for the thermal modes Y_1, Z_1, Y_2, Z_2 etc., being the middle $K-2$ entries. In general this set of K ordinary differential equations is a high-order coupled system. If the heat transfer coefficient had been constant in θ, instead of discontinuous at $\theta = 0$ and $\theta = \pi$, the summation terms due to thermal 'cross-diffusion' would vanish. The first three equations then decouple from the rest and completely determine the flow $X(t)$ as in [3]. However, for the present 'mixed boundary' case the exact splitting into master and slaved problems is not possible. This point was noted by Sen *et al.* [7] who looked in detail at a situation where $H(\theta)$ is given all around the loop and h and A are identically zero. Their case does decouple to 3 modes, but, because there is no axial nor wall heat conduction, is somewhat unrealistic. If axial conduction is included, however, their model becomes equivalent to that in [3] if h_0 is set equal to $kR_p/2R_0^2$.

Thus the three-component (3 ODE) model of [3] does not strictly apply to cases where h varies. The situation studied here reflects a very severe variation of $h(\theta)$. It is the purpose of this note to investigate how well an approximate low-mode model predicts the dynamics and in the process to show some long-time characteristics of the full solutions. Most of the interesting motions (instability, oscillations, substantial steady flows, etc.) occur at moderate to large Rayleigh number Ra. Since the coupling terms [the sums in equations (6)–(9)] arise from conduction effects, which are weak at large Ra, we expect that a three- or four-component version of these equations may indeed accurately forecast the dynamic behavior of the system.

The $K = 4$ subset of the model equations is shown below:

$$\frac{dX}{dt} = Pr[-X + \cos(\alpha)Y - \sin(\alpha)(Z - Ra)] \tag{10}$$

$$\frac{dY}{dt} = -XZ + Ra\, X - Y \tag{11}$$

$$\frac{dZ}{dt} = XY - Z - y_0 \tag{12}$$

$$\frac{dy_0}{dt} = \left(-y_0 - \frac{8Z}{\pi^2}\right) \tag{13}$$

where we have written (Y, Z) for (Y_1, Z_1). Since $A \ll 1$ the $(1+2A)$ terms in (13) have been replaced by 1s. It may be noted that equations (10)–(12) are identical to equations (11)–(13) of [3] if $y_0 = 0$. Of course if h is uniform, the last term of equation (13) above is zero and y_0 does decay to zero. In the current situation, a proper determination of the steady solutions requires that we include this one additional equation for the mean temperature.

Steady solutions of the subset are given by

$$X_0^3 + bX_0[1 - \cos(\alpha)\, Ra] - b \sin(\alpha)\, Ra = 0 \tag{14a}$$

$$Y_0 = Ra\frac{X_0}{(X_0^2/b) + 1} \tag{14b}$$

$$Z_0 = \frac{X_0 Y_0}{b}. \tag{14c}$$

As in [3] equation (14a) admits multiple real solutions for $\alpha = 0$ and some $\alpha > 0$. For $\alpha = 0$, the non-zero solutions are $X_0 = \pm[b(Ra-1)]^{1/2}$. Working back through the transformation one finds that

$$v'^2 = \frac{4Ra'}{\pi} - \frac{b}{4}. \tag{15}$$

Equations (3) and (4) can be solved exactly for steady motion. Under the present circumstances with α and A zero, we find

$$v'^2 = \frac{2Ra'}{\pi} + \frac{v' Ra'}{(v'^2+1)\tanh\left(\frac{\pi}{2v'}\right)} \tag{16}$$

These two results are compared in Fig. 2. It is seen that except for very small Ra' the two curves are almost identical. In fact, at small Ra' the 'exact' result of equation (16) is pathological since if a small amount of axial conduction is included the velocity goes to zero at a finite Ra'. This is in fact predicted by the low-order model since it has a zero root which is stable for $Ra < 1.0$. It can be shown that the low-mode model also works well for non-zero α less than about 45°. This is the range of interest here since at large α the steady flows are extremely stable. Thus our hypothesis that the low-mode model is useful for interesting values of Ra and α is supported by this test.

The stability of the steady motions are investigated by perturbing equations (10)–(13) about the fixed-point solutions given by equation (14). If equation (13) is omitted from the stability calculations simple analytic formulae for the neutral curves can be found. These correspond to a three-mode stability analysis of the $K = 4$ steady solutions. At $\alpha = 0$ the steady flows are predicted to become unstable when the Rayleigh number crosses the threshold value given by

$$Ra_c = \left[1 + \frac{(Pr+2)(Pr+1)}{b(Pr-2)}\right]. \tag{17}$$

Figures 3(a)–3(d) show bifurcation diagrams for several cases. These can be compared qualitatively with Figs. 5–7 of [3], although the previous analysis corresponded to $b = 1.0$ and, as pointed out earlier, does not apply to the present situation.

As Ra is increased past the critical value one expects solution trajectories to move away from an unstable branch and onto another steady branch if it exists and is attracting. If there are no stable steady branches, periodic or chaotic motion should ensue. Figure 3(e) shows one plot using the full subset ($K = 4$) for the stability calculation. There is an anomalous region of instability on the lower branch that disappears at higher K. In fact, at large K the diagrams resemble those in Figs. 3(a)–(d) very closely. Table 1 compares some critical points from the different models. In this table column 3 is from equation (17), column 4 is obtained by solving the quartic stability equation for

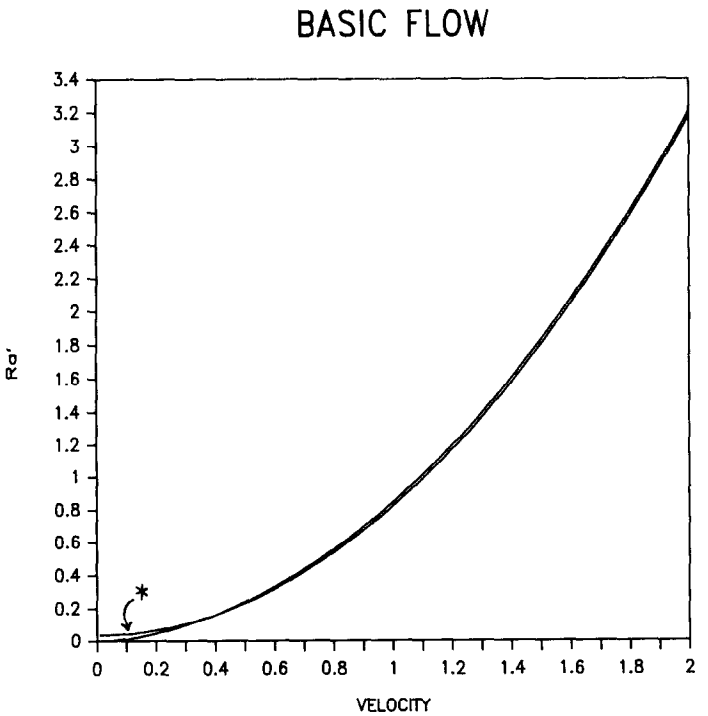

FIG. 2. Comparison of steady flow predictions: * four-mode model; —— full solution without axial diffusion.

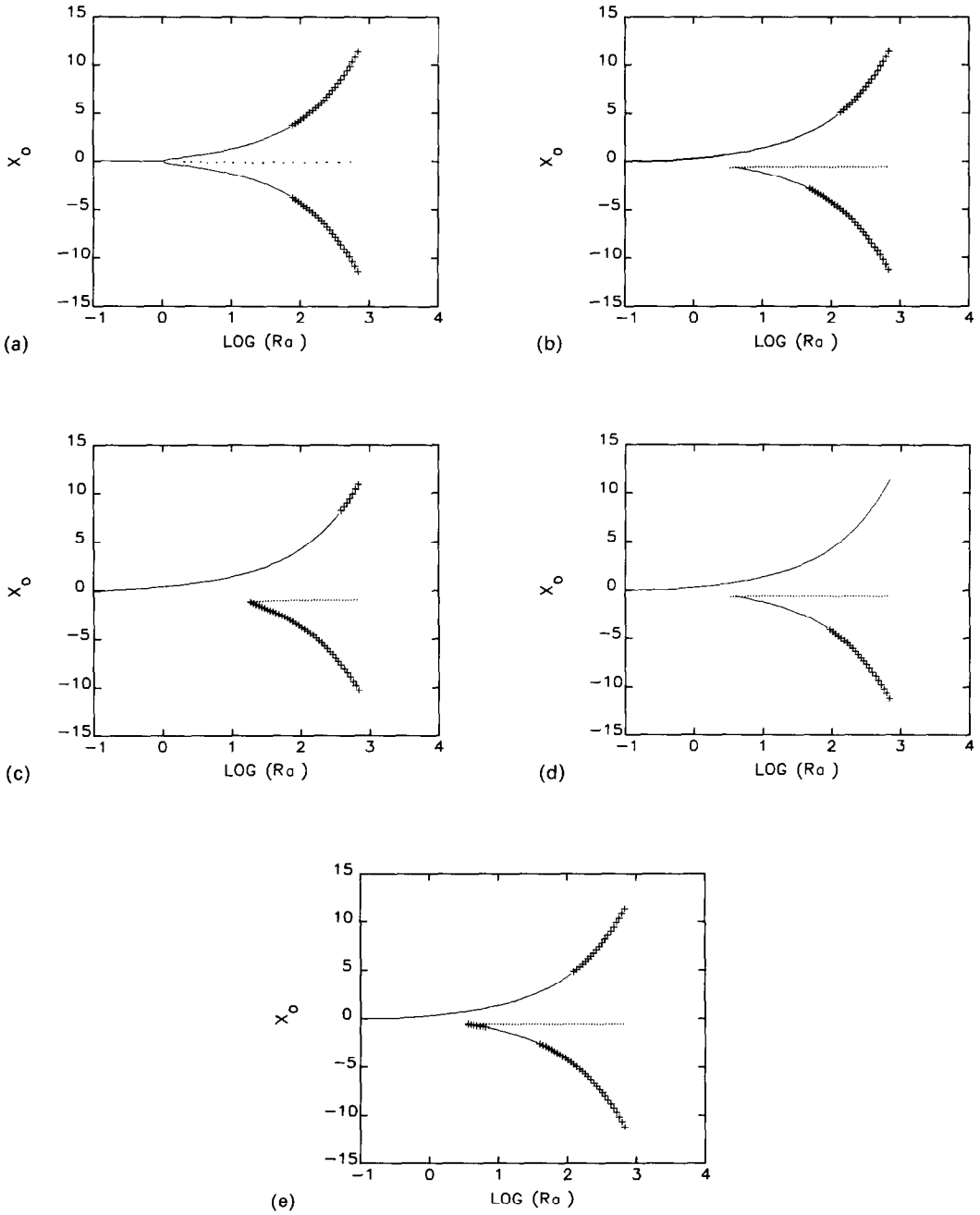

FIG. 3. Three-mode stability plots [except 3(e) which has $K = 4$]. Solid lines are stable, cross-hatched points are overstable, and dots are monotonically unstable fixed-points: (a) $Pr = 7.0, \alpha = 0$; (b) $Pr = 7.0, \alpha = 10°$; (c) $Pr = 7.0, \alpha = 30°$; (d) $Pr = 50.0, \alpha = 10°$; (e) $Pr = 10.0, \alpha = 10°$.

the $K = 4$ sub-model, and column 5 represents results of numerical initial value problems. It is seen that the critical values from all the models are within about 5%.

3. NUMERICAL RESULTS

To illustrate the behavior of the full model for these mixed boundary conditions, and to further test the usefulness of the low-dimensional model outlined above, we compare numerical solutions of equations (6)–(9) at high K with the low K stability results and $K = 4$ numerical solutions. Equation (13) must be included in the lowest resolution numerical model if one wants to study migration from one steady branch to another where y_0 changes substantially. Solutions are calculated using a 4th order Runge–Kutta scheme. The time step depends on K but is typically 0.01. Runs of order 10^5 steps are made. Convergence was tested by doubling the truncation level K and requiring that the solution be essentially unchanged. In some instances

Table 1. Critical Ra for the upper branch of steady solutions

α (degrees)	Pr	Three-mode*	$K = 4$	$K = 40$
0	7.0	77.2	72.5	77.0
0	30.0	188.5	185.7	188.5
0	3.0	106.2	94.6	104.5
10	7.0	126.3	122.3	124.0
10	30.0	480.2	478.5	479.0
10	3.0	167.6	154.5	158.0

* But using the steady solution determined from the $K = 4$ sub-model.

when A was very small, moderate truncation (e.g. $K = 12$) gave spurious results that were not found at larger K. For example at $Ra = 78$, $\alpha = 0$, $Pr = 7$, $A = 0.001$ doubly-periodic solutions (motion on a two-torus) at $K = 12$ gave way to low-dimensional chaos at $K = 28$. The reason for this behavior is that solutions of the equations with no axial conduction have discontinuous derivatives in temperature. These of course are anomalous, and cannot be represented by the expansion (4b). For the problem to make physical sense, and for numerical practicality, a modest amount of axial heat conduction must be included. We take $A \gtrsim 0.01$ here. This means that the aspect ratio of the torus R_p/R_o is about 0.1.

It was first verified that the transition points given in Fig. 3 are almost exactly reproduced by the full calculations. Specific examples are given in Table 1, but in general the steady branches become unstable within a few percent of the Ra values predicted by the three-component stability problem. In addition, the nature of the ensuing motions are nearly equivalent.

Figure 4 shows the initial part of a $K = 40$ time trace at a Rayleigh number just above the bifurcation point at $Ra = 77.2$ given in Fig. 3(a). The motion evolves onto a chaotic attractor similar to that of Lorenz [2]. Several orbits are shown in phase space projection in Fig. 5(a). This is made by plotting the velocity variable $X(t)$ against itself $X(t+t'')$ lagged forward in time by a constant displacement t''. Figure 5(b) shows the trajectories of the three-component model. The orbits are not identical at the same time in the two runs

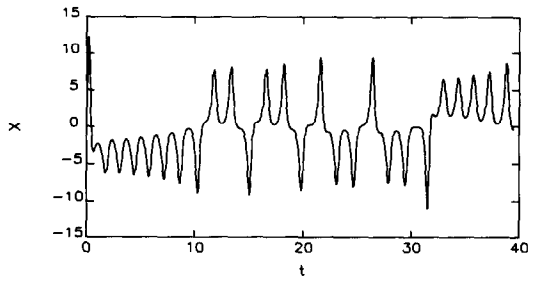

FIG. 4. Time trace of velocity for $Ra = 80.0$, $Pr = 7.0$, $A = 0.01$, $\alpha = 0$, $K = 40$.

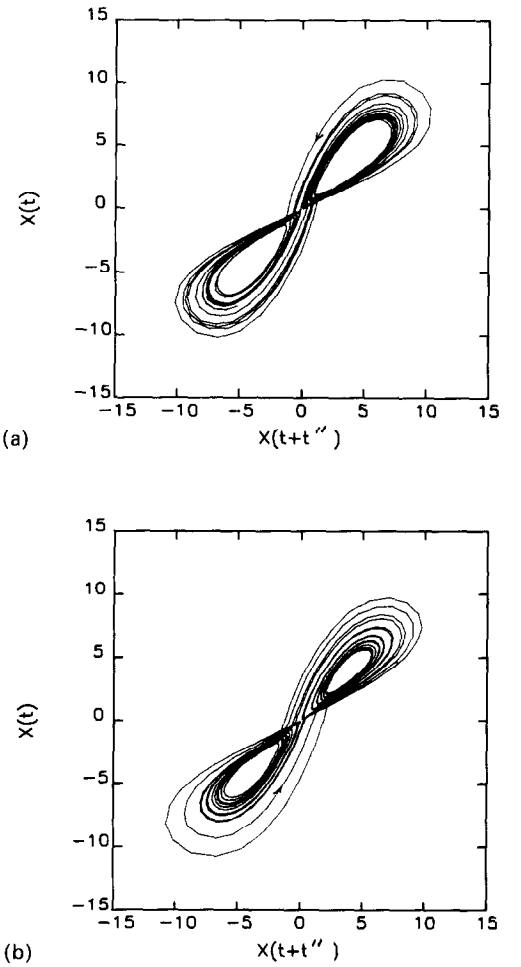

FIG. 5. Chaotic phase portraits for $\alpha = 0$, $Pr = 7.0$, $Ra = 80.0$. (a) $K = 40$, $A = 0.01$; (b) $K = 4$, $A = 0.01$.

because these chaotic solutions are very sensitive to small changes in initial conditions (and thus to small truncation effects), but the attractors appear to be topologically equivalent. This is however not exactly true. Chaotic solutions of the three-component model have the interesting property, originally discovered by Lorenz [2], that the points of an iterative map obtained by plotting successive maxima of the Z variable against the previous maxima fall nearly on a curve. One such map is shown in Fig. 6(a). The details of the chaotic motion appear much more clearly here than in phase space projection, and such maps have been extensively studied (see [8]) to gain insight into the nature and origin of the chaotic dynamics. Figure 6(b) shows a map for $K = 40$ (the map for $K = 26$ is the same). Although the two maps are similar, they are not exactly identical, the one in (b) being double peaked. The points do still fall close to a pair of curves indicating low-dimensional chaos. The difference between the two is rather subtle, and it would take a very clean experimental data set to distinguish them unambiguously.

The double-peaked map is a result of the variation of

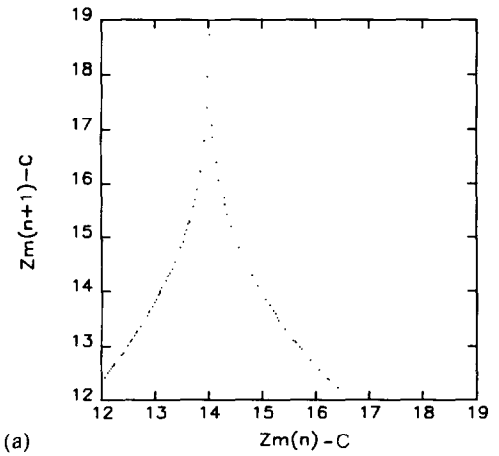

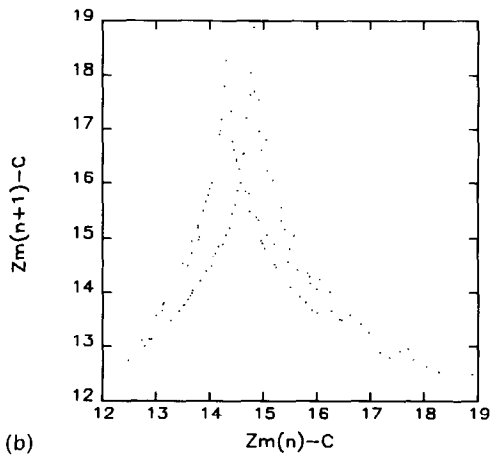

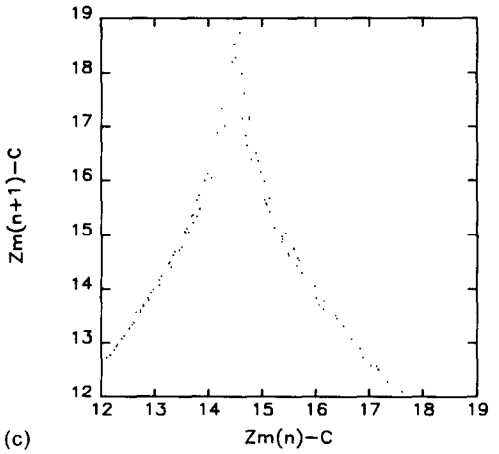

FIG. 6. Plots of maxima of $Z_1 \equiv Z_m$ against previous maxima. $Ra = 80.0$, $Pr = 7.0$, $\alpha = 0$, $C = 70.0$. (a) $K = 4$, $A = 0.01$; (b) $K = 40$, $A = 0.01$; (c) $K = 28$, $A = 0.05$.

heat transfer coefficient, or mathematically a result of the participation of higher thermal modes. The mode power spectrum has substantial contributions from $m = 1$, 2 and 3, decreasing by 10^{-6} at $m = 18$. When the axial conduction is increased the higher θ-modes

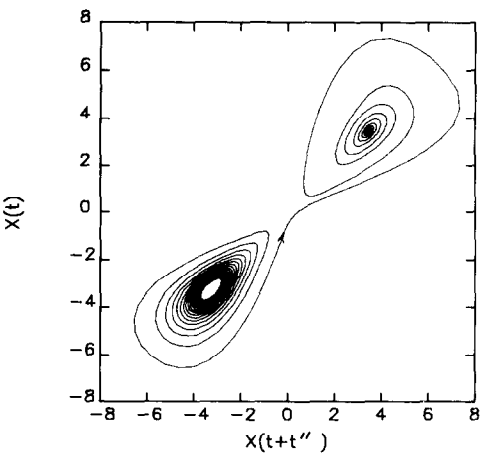

FIG. 7. Phase plot of a solution leaving the unstable clockwise fixed-point. $Ra = 60.0$, $K = 40$, $\alpha = 10°$, $Pr = 7.0$.

are suppressed and the two peaks merge into one, more closely resembling the Lorenz map [Fig. 6(c)].

Figure 7 shows how a solution started near the unstable lower root for $\alpha = 10°$ spirals out to the other attracting stable fixed point. However, when Ra is greater than 126.4 this upper steady motion, which is in direct response to the sideways component of the heating, loses its stability and chaotic motion again begins. This is shown in Fig. 8. In Fig. 9 the projected attractors at high and low truncation can again be compared. This chaotic motion is biased so that it spends most of its time near the least unstable fixed-point. Figure 10 displays iterative mappings generated from two models. Although the maps are similar, there are still some subtle differences as in the previous case.

Numerical calculations also show that the Hopf bifurcations are inverted. For example, a solution started at $Ra = 121$, e.g. below the bifurcation point but with an initial condition far from the steady fixed-point, goes chaotic. On the other hand solutions at the same parameter settings but with initial values close to the fixed-point given by equations (14) spiral into that fixed-point.

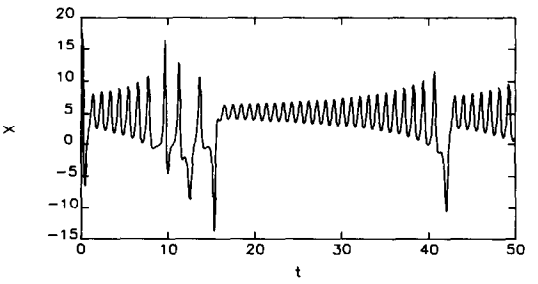

FIG. 8. Time trace for $Ra = 135.0$, $\alpha = 10°$, $Pr = 7.0$, $A = 0.01$, $K = 40$.

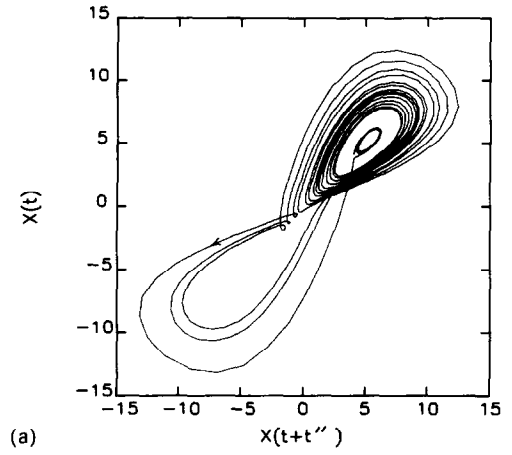

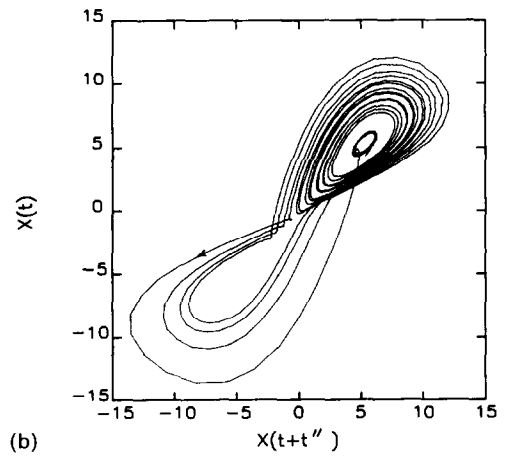

FIG. 9. Attractors for same conditions as in Fig. 8 except (a) $K = 40$; (b) $K = 4$.

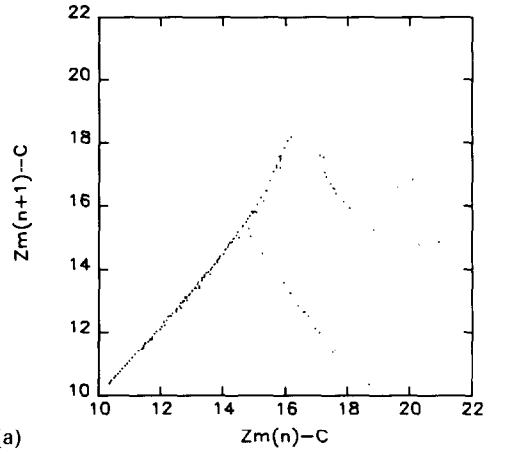

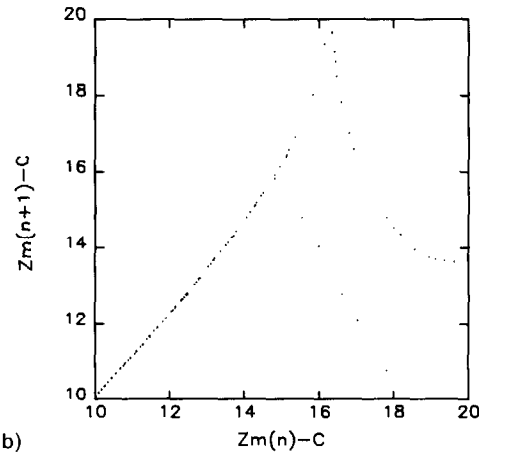

FIG. 10. Maxima maps for $Ra = 135.0$, $A = 0.01$, $Pr = 7.0$, $\alpha = 0$. (a) $K = 40$; (b) $K = 4$.

4. CONCLUSIONS

A low-dimensional model of the loop thermosyphon gives rather accurate predictions of the steady motion, stability and time dependent motions in a case where the heat transfer coefficient is zero for the lower half of the loop, and constant for the upper half. Thus although the Lorenz-like models previously proposed are not exact unless h is uniform over the torus, they do a reasonable job in forecasting the expected time-asymptotic state of motion. Numerical computations with sufficient resolution for convergence suggest that the steady motion breaks down into chaos via a subcritical Hopf bifurcation as the Rayleigh number is increased. The chaotic motion itself is slightly altered by cross-diffusion terms resulting from the discontinuity in the boundary condition at the wall. The structure of the Lorenz cusp maps generated by the chaotic solutions of the four-equation model are roughly preserved although in the full model they appear to be doubly instead of singly peaked. This latter behavior, along with the concomitant multiple curves in the wings of the map, may be responsible for some of the broadening in the experimentally measured map of Gorman *et al.* [6], although noise' induced by three-dimensional secondary motions may also contribute. If our model system is made more dissipative by including a fair amount of axial diffusion, the two peaks in the chaotic map merge into one. This resembles more closely the map produced by the low-order model.

This study reinforces the notion suggested in [3] that there are no purely periodic solutions for reasonably small Ra, only steady or chaotic ones. These flows, and the bifurcations between them, can be quite accurately calculated with a simple model made up of three or four ordinary differential equations.

Acknowledgements—The author would like to thank Dr. Mihir Sen for his helpful comments on this problem and for sending a pre-print of his paper. This research was sponsored by NASA under contract NAS-8-31958.

REFERENCES

1. W. V. R. Malkus, Non-periodic convection at high and low Prandtl number, *Mem. Soc. R. Sci., Liege* **4**, 125–128 (1972).

2. E. N. Lorenz, Deterministic non-periodic flow, *J. atmos. Sci.* **20,** 130–141 (1963).
3. J. E. Hart, A new analysis of the closed loop thermosyphon, *Int. J. Heat Mass Transfer* **27,** 125–136 (1984).
4. H. F. Creveling, J. F. DePaz, J. Y. Baladir and R. J. Schoenhals, Stability characteristics of a single-phase free convection loop, *J. Fluid Mech.* **67,** 65–84 (1975).
5. P. S. Damerell and R. J. Schoenhals, Flow in a toroidal thermosyphon with angular displacements of heated and cooled sections, *J. Heat Transfer* **101,** 672–676 (1979).
6. M. Gorman, P. J. Widmann and K. A. Robbins, Chaotic flow regimes in a convection loop. *Phys. Rev. Lett.* **52,** 2241–2244 (1984).
7. M. Sen, E. Ramos and C. Trevino, The toroidal thermosyphon with a known heat flux, *Int. J. Heat and Mass Transfer* **28,** 219–233 (1985).
8. C. Sparrow, *The Lorenz Equations: Bifurcations, Chaos and Strange Attractors.* Appl. Mathematics and Science, Vol. 41. Springer, New York (1982).

NOTE SUR UNE BOUCLE DE THERMOSIPHON AVEC DES CONDITIONS AUX LIMITES MIXTES

Résumé—On présente un modèle monodimensionnel d'écoulement dans une boucle toroïdale de fluide dans laquelle le coefficient de transfert thermique pariétal est constant sur une moitié de la boucle et nul sur l'autre. Une forme mathématique du modèle donne des prévisions raisonnablement précises du débit masse permanent, de la stabilité et de la nature des mouvements variables. Des calculs numériques avec un modèle hautement dimensionnel illustre les effets des conditions mixtes et de la conduction thermique axiale sur les solutions chaotiques. Des comparaisons sont faites avec les modèles faiblement dimensionnels qui sont exacts seulement pour un coefficient de transfert thermique spatialement uniforme.

DER SCHLEIFEN-THERMOSYPHON MIT GEMISCHTEN RANDBEDINGUNGEN

Zusammenfassung—Für die Strömung in einem torusförmigen Fluidkreislauf, bei dem der Wärmeübergangs-Koeffizient in der einen Hälfte konstant, in der anderen null ist, wird ein eindimensionales Modell vorgeschlagen. Ein derartiges mathematisches Modell von kleiner Dimension führt zu einer recht genauen Vorausberechnung des stationären Massenstroms, der Stabilität und der Natur der instationären Bewegungen. Numerische Berechnungen mit einem Modell von großer Dimension verdeutlichen den Einfluß der gemischten Randbedingungen und der axialen Wärmeleitung auf die chaotischen Lösungen. Vergleiche werden mit früheren Modellen von kleiner Dimension angestellt, welche exakt nur für einen insgesamt konstanten Wärmeübergangskoeffizienten gelten.

О СМЕШАННЫХ ГРАНИЧНЫХ УСЛОВИЯХ ДЛЯ ТЕРМОСИФОНА, ИМЕЮЩЕГО ФОРМУ ПЕТЛИ

Аннотация—Представлена одномерная модель течения в тороидальной петле жидкости, у которой в одной половине петли коэффициент теплообмена стенки постоянен, а в другой равен нулю. Математическая модель с низкой размерностью позволяет с разумной точностью рассчитать стационарный поток, проанализировать устойчивость и природу неустановившихся движений. Численные расчеты модели бóльшей размерности выявляют воздействие смешанных границ и аксиальной теплопроводности на хаотические решения. Результаты сравниваются с результатами для моделей с низкой размерностью, которые являются точными только для постоянного коэффициента теплообмена.